WARSAW UNIVERSITY OF TECHNOLOGY Index 351733
FACULTY OF CIVIL ENGINEERING
COMMITTEE FOR CIVIL AND WATER ENGINEERING
POLISH ACADEMY OF SCIENCES ISSN 1230-2945
DOI: 10.24425/ace.2024.151911
ARCHIVES OF CIVIL ENGINEERING
Vol. LXX ISSUE 4 2024
pp. 579 –597

Research paper

Impact coefficient of tied arch bridges considering heavy transport vehicles

Shu-Qi He[1], De-Jian Li[2]

Abstract: Analyzing the impact coefficient of tied arch bridges considering heavy transport vehicles is important for safety assessment. There are few studies on the vehicle-bridge coupled dynamic analysis involving heavy transport vehicles passing through bridges. In order to properly evaluate the impact coefficient of heavy transport vehicles passing through tied-arch bridges, this study takes an 80 m-span tied-arch bridge as an example. Based on the ANSYS platform, a vehicle-bridge coupling model under the load of low-speed heavy transport vehicles is established. By analyzing the vibration characteristics of the vehicle-bridge coupling system, the influence of vehicle speed and load on the impact coefficient of the bridge is discussed. The results show that even when the vehicle travels at a speed of 2 m/s under Class B roughness, the maximum impact coefficient reaches 0.061 when the vehicle is 4 m/s. When evaluating the passage of heavy transport vehicles over tied-arch bridges, the impact effect should be considered even at low speeds. The influence of vehicle load on the internal force impact coefficient of tied-arch bridges is greater than that of the displacement impact coefficient. When the vehicle load is large, the impact on the bridge is small, but an excessive increase in vehicle load will increase the burden on the bridge. A load of 400 t is considered a more ideal value.

Keywords: heavy transport, tied-arch bridge, vehicle-bridge coupling vibration, impact coefficient

[1]BSC., Eng., Department of Bridge Engineering, School of Civil Engineering, Central South University, Changsha, Hunan, 410075, China, e-mail: 995787343@qq.com, ORCID: 0009-0005-7196-926X
[2]Prof., DSc., PhD., Eng., Department of Bridge Engineering, School of Civil Engineering, Central South University, Changsha, Hunan, 410075, China, e-mail: heshuqi_2023@163.com, ORCID: 0009-0003-4567-675X

1. Introduction

Highway heavy transport refers to the use of special vehicles for the transportation of special goods that are overweight, oversized, over-width, and over-height by road vehicles [1–3]. With the rapid development of China's economy, industry, and new energy industry, there has been an increasing number of transportation activities involving heavy and non-detachable objects such as transformers, wind turbine blades, and reactors. The load of heavy transport vehicles far exceeds that of overloaded vehicles. These vehicles usually pass through bridges at lower speeds to reduce dynamic responses. However, the impact effects on bridges still exist, and their dynamic response characteristics are also unique [4–8]. Simply applying the method of using impact coefficients for standard cars is not appropriate. Therefore, it is imperative to establish a reasonable and effective vehicle-bridge coupled vibration model under low-speed conditions for heavy transport vehicles, accurately measure the dynamic effects of highway heavy transport vehicles, and provide a basis for safety assessment.

Currently, there have been numerous studies on the vehicle-bridge coupled dynamic analysis of tied-arch bridges, both domestically and internationally. Zhang et al. developed a vehicle-bridge coupling vibration program to analyze the dynamic response of a steel tube reinforced concrete tied-arch bridge [9]. Zeng et al. proposed the "matching" principle and the principle of constant potential energy for elastic systems [10, 11]. Yin established a finite element model of a large-span steel box girder tied-arch bridge based on the principle of constant potential energy for elastic systems and the formation matrix of the "matching" principle, analyzing the influence of temperature deformation on the dynamic response of the vehicle-bridge system [12]. Chen and Cai considered the influence of wind and established a wind-vehicle-bridge coupling model [13]. Zhu et al. proposed a method for analyzing the random dynamic stress of suspension rods using the vehicle-line-bridge coupling dynamics and virtual excitation method, studying the non-uniformity of the stress impact coefficient at different positions of the suspension rods and analyzing the influence of vehicle speed and track unevenness on the stress impact coefficient [14]. Paolo quantitatively and numerically studied the dynamic amplification factors of displacement and stress by parameterizing the structural features of bridges and moving loads, using the finite element method to establish basic formulas, evaluating the coupling effects between bridge deformations and moving loads, and proposing a sensitivity analysis method based on dynamic influence factors [15]. Jang analyzed the dynamic interaction between tied-arch bridges and trains, proposing two resonance conditions [16]. However, there are relatively few studies on the vehicle-bridge coupled dynamic analysis involving heavy transport vehicles passing through bridges, making it particularly important to investigate the dynamic response of such vehicles to bridges.

This study focuses on a tied-arch bridge with an 80 m span. The vehicle chosen is a commonly used bridge-type frame truck for highway heavy transport. Utilizing the ANSYS software, a heavy transport vehicle-bridge coupling vibration solving model is established using the principle of constant potential energy and the constraint equation method. The influence of bridge stiffness, bridge deck roughness, vehicle speed, vehicle load, spring stiffness and damping in the vehicle suspension system, and bridge damping ratio on bridge dynamic response and dynamic amplification factors are discussed.

2. Model establishment

2.1. Vehicle model

Based on the principle of constant potential energy for elastic systems, taking the static equilibrium position of the vehicle as the reference position and a $n + n$ axle bridge-type frame truck as an example, the dynamic balance equations are derived. Fig. 1 shows a schematic diagram of the bridge-type frame truck.

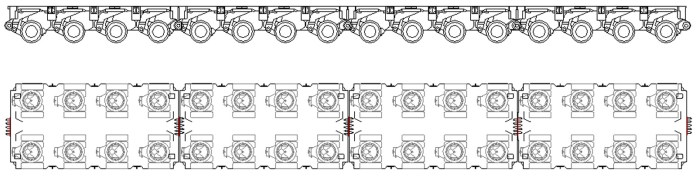

Fig. 1. A schematic diagram of the bridge-type frame truck

Figs. 2 and 3 represent the simplified model of the n+n axle twin-column bridge-type frame truck, which is simplified to three rigid body spring-mass-damper systems. The entire vehicle

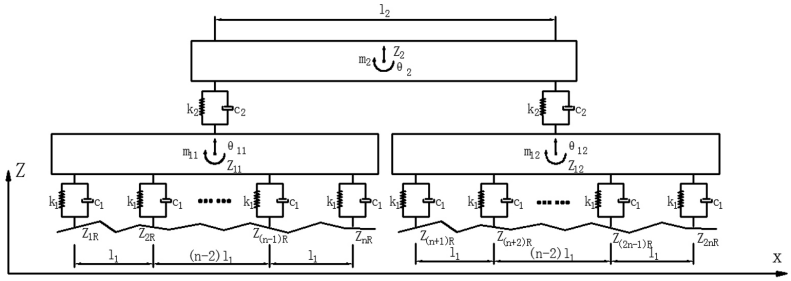

Fig. 2. Front view of the simplified model of the n+n axle twin-column bridge-type frame truck

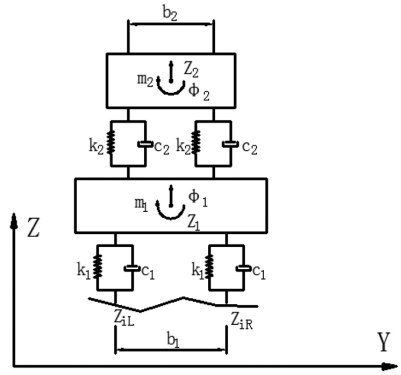

Fig. 3. Side view of the simplified model of the n+n axle twin-column bridge-type frame truck

has a total of 4n endpoints and 9 degrees of freedom. The three rigid bodies (represented by three rectangles) correspond to the load-bearing beam of the bridge-type frame truck and the front and rear traveling mechanisms (including the uniformly loaded beam and the hydraulic flatbed truck) on both sides. Let m_2 be the mass of the load-bearing beam, m_{11} be the mass of the front traveling mechanism, and m_{12} be the mass of the rear traveling mechanism. k_1 and c_1 represent the equivalent spring stiffness and damping (first series spring stiffness and damping) of the suspension structure of the hydraulic flatbed truck in the traveling mechanism of the bridge-type frame truck. k_2 and c_2 represent the equivalent spring stiffness and damping (second series spring stiffness and damping) between the load-bearing beam and the front and rear traveling mechanisms of the bridge-type frame truck. l_1 represents the distance between the axles. l_2 represents the effective span of the load-bearing beam. b_1 represents the distance between the tires on the same axle. b_2 represents the distance of the jacking cylinder of the load-bearing beam.

Assuming that at the static equilibrium position of the vehicle, θ, φ, Z, and the deflection of the bridge are all small quantities, and the bridge-type frame truck always stays in contact with the bridge during travel, we have:

$$Z_i = Z(t, x_i, y_i) + Z_{iRo} \tag{2.1}$$

where $Z(t, x_i, y_i)$ represents the deflection of the bridge corresponding to the ith wheel at time t, with downward direction as negative; Z_{iRo} represents the roughness value of the bridge deck, with upward direction as positive.

The dynamic balance equations of the entire vehicle are as follows:

$$[M]\{\ddot{Z}\} + [C]\{\dot{Z}\} + [K]\{Z\} = \{P\} \tag{2.2}$$

where $[M]$, $[C]$, and $[K]$ represent the mass, damping, and stiffness matrices of the vehicle; $\{P\}$ represents the column vector of external forces acting on the vehicle; $\{\ddot{Z}\}$, $\{\dot{Z}\}$, and $\{Z\}$ represent the acceleration, velocity, and displacement vectors of the vehicle.

The mass matrix of the vehicle model is given by:

$$[M] = \operatorname{diag}[m_2, J_{\theta 2}, J_{\varphi 2}, m_{11}, J_{\theta 11}, J_{\varphi 11}, m_{12}, J_{\theta 12}, J_{\varphi 12}] \tag{2.3}$$

where $J_{\theta 2}$ is the moment of inertia of the bridge beam, $J_{\varphi 2}$ is the tilt moment of inertia of the bridge beam, $J_{\theta 11}$ and $J_{\theta 12}$ are the moment of inertia of the traveling mechanism, $J_{\varphi 11}$ and $J_{\varphi 12}$ are the tilt moment of inertia of the traveling mechanism.

I. When n is even, $a = n/2$, the elements of the $[K]$ matrix are as follows:

$$[K] = \begin{bmatrix}
4k_2 & 0 & 0 & -2k_2 & 0 & 0 & -2k_2 & 0 & 0 \\
0 & l_2^2 k_2 & 0 & -l_2 k_2 & 0 & 0 & l_2 k_2 & 0 & 0 \\
0 & 0 & 4b_2^2 k_2 & 0 & 0 & 0 & 0 & 0 & 0 \\
-2k_2 & -l_2 k_2 & 0 & 2k_2 + (4a+2)\,k_1 & 0 & 0 & 0 & 0 & 0 \\
0 & 0 & 0 & 0 & \tfrac{1}{3}a(a+1)(2a+1)l_1^2 k_1 & 0 & 0 & 0 & 0 \\
0 & 0 & 0 & 0 & 0 & 4ab_1^2 k_1 & 0 & 0 & 0 \\
-2k_2 & l_2 k_2 & 0 & 0 & 0 & 0 & 2k_2 + (4a+2)k_1 & 0 & 0 \\
0 & 0 & 0 & 0 & 0 & 0 & 0 & \tfrac{1}{3}a(a+1)(2a+1)l_1^2 k_1 & 0 \\
0 & 0 & 0 & 0 & 0 & 0 & 0 & 0 & 4ab_1^2 k_1
\end{bmatrix}$$

The elements of the $[C]$ matrix are as follows:

$$[C]=\begin{bmatrix}
4c_2 & 0 & 0 & -2c_2 & 0 & 0 & -2c_2 & 0 & 0\\
0 & l_2^2c_2 & 0 & -l_2c_2 & 0 & 0 & l_2c_2 & 0 & 0\\
0 & 0 & 4b_2^2c_2 & 0 & 0 & 0 & 0 & 0 & 0\\
-2c_2 & -l_2c_2 & 0 & 2c_2+(4a+2)\,c_1 & 0 & 0 & 0 & 0 & 0\\
0 & 0 & 0 & 0 & \frac{1}{3}a(a+1)(2a+1)l_1^2c_1 & 0 & 0 & 0 & 0\\
0 & 0 & 0 & 0 & 0 & 4ab_1^2c_1 & 0 & 0 & 0\\
-2c_2 & l_2c_2 & 0 & 0 & 0 & 0 & 2k_2+(4a+2)c_1 & 0 & 0\\
0 & 0 & 0 & 0 & 0 & 0 & 0 & \frac{1}{3}a(a+1)(2a+1)l_1^2c_1 & 0\\
0 & 0 & 0 & 0 & 0 & 0 & 0 & 0 & 4ab_1^2c_1
\end{bmatrix}$$

The elements of the $\{P\}$ column vector are as follows:

$$\{P\}=\begin{Bmatrix}
0\\
0\\
0\\
\sum\limits_{i=1}^{2a}k_1Z_{R1i}+\sum\limits_{i=1}^{2a}k_1Z_{L1i}\\
\sum\limits_{i=1}^{a}k_1l_1\left(n-\frac{2i-1}{2}\right)Z_{R1i}-\sum\limits_{i=a+1}^{2a}k_1l_1\left(n-\frac{2i-1}{2}\right)Z_{R1i}+\sum\limits_{i=1}^{a}k_1l_1\left(n-\frac{2i-1}{2}\right)Z_{L1i}-\sum\limits_{i=a+1}^{2a}k_1l_1(n-\frac{2i-1}{2})Z_{L1i}\\
\sum\limits_{i=1}^{a}k_1b_1Z_{R1i}+\sum\limits_{i=a+1}^{2a}k_1b_1Z_{R1i}-\sum\limits_{i=1}^{a}k_1b_1Z_{L1i}-\sum\limits_{i=a+1}^{2a}k_1b_1Z_{L1i}\\
\sum\limits_{i=1}^{2a}k_1Z_{R2i}+\sum\limits_{i=1}^{2a}k_1Z_{L2i}\\
\sum\limits_{i=1}^{a}k_1l_1\left(n-\frac{2i-1}{2}\right)Z_{R1i}-\sum\limits_{i=a+1}^{2a}k_1l_1\left(n-\frac{2i-1}{2}\right)Z_{R1i}+\sum\limits_{i=1}^{a}k_1l_1\left(n-\frac{2i-1}{2}\right)Z_{L1i}-\sum\limits_{i=a+1}^{2a}k_1l_1\left(n-\frac{2i-1}{2}\right)Z_{L1i}\\
\sum\limits_{i=1}^{a}k_1b_1Z_{R2i}+\sum\limits_{i=a+1}^{2a}k_1l_1Z_{R2i}-\sum\limits_{i=1}^{a}k_1l_1Z_{L2i}-\sum\limits_{i=a+1}^{2a}k_1l_1Z_{L2i}
\end{Bmatrix}$$

II. When n is odd, $a=(n-1)/2$, the elements of the $[K]$ matrix are as follows:

$$[K]=\begin{bmatrix}
4k_2 & 0 & 0 & -2k_2 & 0 & 0 & -2k_2 & 0 & 0\\
0 & l_2^2k_2 & 0 & -l_2k_2 & 0 & 0 & l_2k_2 & 0 & 0\\
0 & 0 & 4b_2^2k_2 & 0 & 0 & 0 & 0 & 0 & 0\\
-2k_2 & -l_2k_2 & 0 & 2k_2+4ak_1 & 0 & 0 & 0 & 0 & 0\\
0 & 0 & 0 & 0 & \frac{1}{3}a\left(4a^2-1\right)l_1^2k_1 & 0 & 0 & 0 & 0\\
0 & 0 & 0 & 0 & 0 & 4ab_1^2k_1 & 0 & 0 & 0\\
-2k_2 & l_2k_2 & 0 & 0 & 0 & 0 & 2k_2+4ak_1 & 0 & 0\\
0 & 0 & 0 & 0 & 0 & 0 & 0 & \frac{1}{3}a(4a^2-1)l_1^2k_1 & 0\\
0 & 0 & 0 & 0 & 0 & 0 & 0 & 0 & 4ab_1^2k_1
\end{bmatrix}$$

The elements of the $[C]$ matrix are as follows:

$$[C] = \begin{bmatrix} 4c_2 & 0 & 0 & -2c_2 & 0 & 0 & -2c_2 & 0 & 0 \\ 0 & l_2^2 c_2 & 0 & -l_2 c_2 & 0 & 0 & l_2 c_2 & 0 & 0 \\ 0 & 0 & 4b_2^2 c_2 & 0 & 0 & 0 & 0 & 0 & 0 \\ -2c_2 & -l_2 c_2 & 0 & 2c_2 + 4ac_1 & 0 & 0 & 0 & 0 & 0 \\ 0 & 0 & 0 & 0 & \frac{1}{3}a(4a^2-1)l_1^2 c_1 & 0 & 0 & 0 & 0 \\ 0 & 0 & 0 & 0 & 0 & 4ab_1^2 c_1 & 0 & 0 & 0 \\ -2c_2 & l_2 c_2 & 0 & 0 & 0 & 0 & 2k_2 + 4ac_1 & 0 & 0 \\ 0 & 0 & 0 & 0 & 0 & 0 & 0 & \frac{1}{3}a(4a^2-1)l_1^2 c_1 & 0 \\ 0 & 0 & 0 & 0 & 0 & 0 & 0 & 0 & 4ab_1^2 c_1 \end{bmatrix}$$

The elements of the $\{P\}$ column vector are as follows:

$$\{P\} = \begin{Bmatrix} 0 \\ 0 \\ 0 \\ \sum_{i=1}^{2a+1} k_1 Z_{R1i} + \sum_{i=1}^{2a+1} k_1 Z_{L1i} \\ \sum_{i=1}^{a} k_1 l_1 [(n+1)-i] Z_{R1i} - \sum_{i=a+2}^{2a+1} k_1 l_1 [(n+1)-i] Z_{R1i} + \sum_{i=1}^{a} k_1 l_1 [(n+1)-i] Z_{L1i} - \sum_{i=a+2}^{2a+1} k_1 l_1 [(n+1)-i] Z_{L1i} \\ \sum_{i=1}^{a} k_1 b_1 Z_{R1i} + \sum_{i=a+1}^{2a+1} k_1 b_1 Z_{R1i} - \sum_{i=1}^{a} k_1 b_1 Z_{L1i} - \sum_{i=a+1}^{2a+1} k_1 b_1 Z_{L1i} \\ \sum_{i=1}^{2a+1} k_1 Z_{R2i} + \sum_{i=1}^{2a+1} k_1 Z_{L2i} \\ \sum_{i=1}^{a} k_1 l_1 [(n+1)-i] Z_{R1i} - \sum_{i=a+2}^{2a+1} k_1 l_1 [(n+1)-i] Z_{R1i} + \sum_{i=1}^{a} k_1 l_1 [(n+1)-i] Z_{L1i} - \sum_{i=a+2}^{2a+1} k_1 l_1 [(n+1)-i] Z_{L1i} \\ \sum_{i=1}^{a} k_1 b_1 Z_{R1i} + \sum_{i=a+1}^{2a+1} k_1 b_1 Z_{R1i} - \sum_{i=1}^{a} k_1 b_1 Z_{L1i} - \sum_{i=a+1}^{2a+1} k_1 b_1 Z_{L1i} \end{Bmatrix}$$

This study focuses on a 15+15 axle bridge-type frame truck, with an axle distance of 1.5 m and a lateral wheelbase of 1.8 m. The vehicle in this study is simulated using ANSYS finite element software. The main body (rigid body) of the entire vehicle is simulated using Mpc-184 elements. The mass and moment of inertia of the vehicle body are simulated using Mass-21 mass elements. The spring-damper structure is simulated using Combin-14 elements. The parameters of the bridge-type frame truck are shown in Table 1. In Table 1, the mass of the

Table 1. Parameters of the 15 + 15 axle bridge-type frame truck

Parameter	**Value**	**Parameter**	**Value**
m_2 (kg)	480000	$m_{11,12}$ (kg)	80000
$J_{\theta 2}$ (kg · m^{-2})	9000000	$J_{\varphi 2}$ (kg · m^{-2})	70000
$J_{\theta 11,\theta 12}$ (kg · m^{-2})	10140000	$J_{\varphi 11,12}$ (kg · m^{-2})	180000
l_1 (m)	1.5	l_2 (m)	39.0
b_1 (m)	1.8	b_2 (m)	1.2
k_1 (N · m^{-1})	1200000	k_2 (N · m^{-1})	8044000
c_1 (N · s · m^{-1})	24000	c_2 (N · s · m^{-1})	24000

load-bearing beam, the mass of the front traveling mechanism, the mass of the rear traveling mechanism, the distance between the axles, the effective span of the load-bearing beam, the distance between the tires on the same axle, and the distance of the jacking cylinder of the load-bearing beam are provided by the transport company. Other parameters are determined from the reference [17].

2.2. Bridge model

This study focuses on a medium-span tied-arch bridge with a main span of 80 m, a bridge length of 79.88 m, a hanger spacing of 5.0 m, a bridge width of 35.5 m, and a slenderness ratio of 1/5. We choosing an 80 m bridge because this is a typical span bridge. With this bridge span, we can obtain more general results. The layout of the bridge is shown in Figs. 4 and 5. The material properties of the bridge is listed in Table 2.

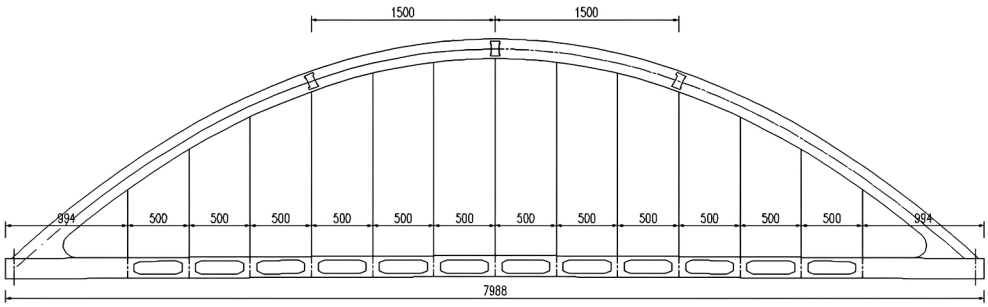

Fig. 4. Front view of the bridge (unit: cm)

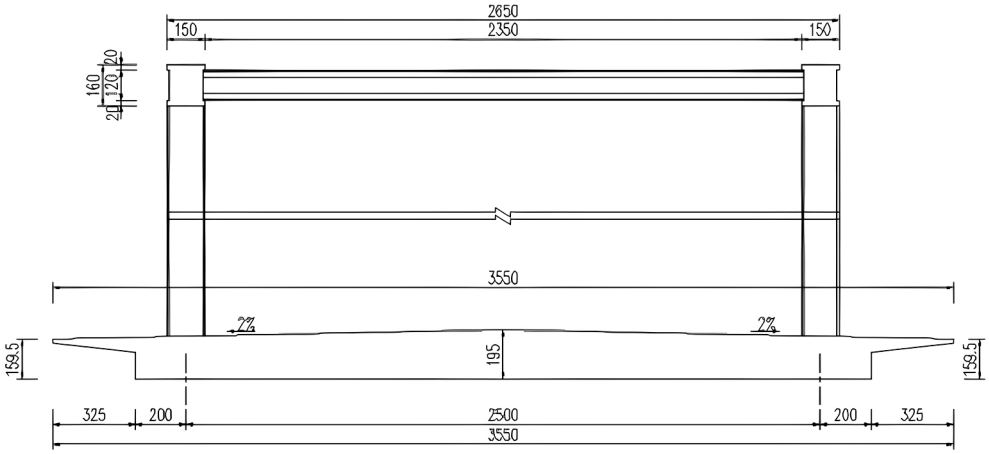

Fig. 5. Side view of the bridge (unit: cm)

Table 2. The material properties of the bridge

Component	Material	Elasticity modulus (GPa)	Density (kg/m^3)	Poisson's ratio
Bridge deck	Concrete	34.5	2600	0.2
Suspender	Steel	195	7850	0.3

The ANSYS finite element software is used to establish the finite element model of the background bridge. Beam-188, Shell-181, and Link-180 elements are applied to simulate different parts of the bridge. The arch ribs, transverse bracings, and bridge deck grid are simulated using the Beam-188 element. The bridge deck panel is simulated using the Shell-181 element. The hangers are simulated using the Link-180 element. The same node coupling method is used to couple the bridge deck panels with the beam grid nodes, ensuring that the forces acting on the bridge deck panels are effectively transmitted to the beam grid. The finite element model is shown in Fig. 6.

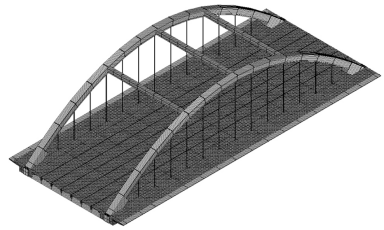

Fig. 6. Finite element model of the bridge

To balance the computational efficiency and accuracy, a mesh convergence analysis is performed first. In the mesh convergence analysis, the bridge model is meshed using three grid resolutions, namely, coarse, medium, and fine. The maximum grid size of the bridge deck in coarse, medium, and fine resolution is approximately 5 m, 3.5 m, and 2 m. Based on the three grid resolutions, the mid-span vertical displacement amplitudes are shown in Fig. 7. As shown

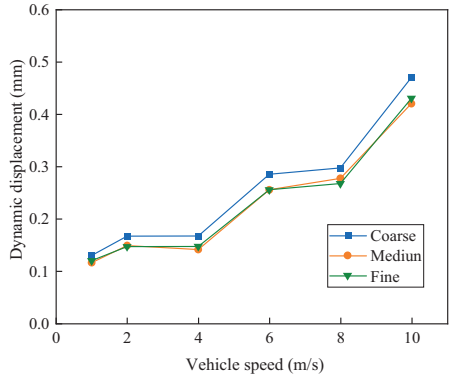

Fig. 7. Mesh convergence analysis

in Fig. 7, the calculation results obtained from the coarse resolution deviates largely from those of medium and fine resolution. The mid-span vertical displacement amplitudes calculated from the models with medium and fine grid resolutions are close. Hence, we finally choose the medium grid resolution for all calculations.

The vibration frequency of first ten modes of the bridge is as listed in Table 3. The first five vibration modes are shown in Fig. 8.

Table 3. Vibration frequency of first ten modes of the bridge

Mode number	**Frequency (Hz)**	**Mode number**	**Frequency (Hz)**
1	0.6618	6	2.7408
2	1.5398	7	3.4765
3	1.7323	8	3.6433
4	2.1091	9	3.7194
5	2.4856	10	3.7614

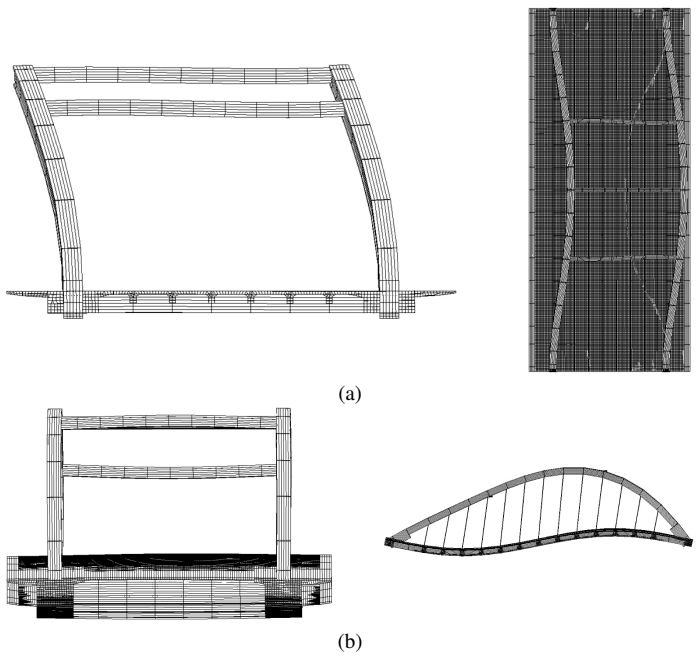

Fig. 8. Vibration mode of the bridge: (a) 1st mode (f = 0.6618 Hz), (b) 2nd mode (f = 1.5398 Hz), (c) 3rd mode (f = 1.7323 Hz), (d) 4th mode (f = 2.1091 Hz), (e) 5th mode (f = 2.4856 Hz)

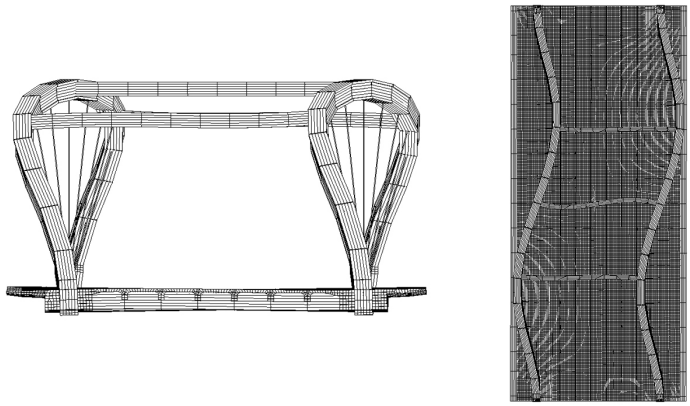

(c)

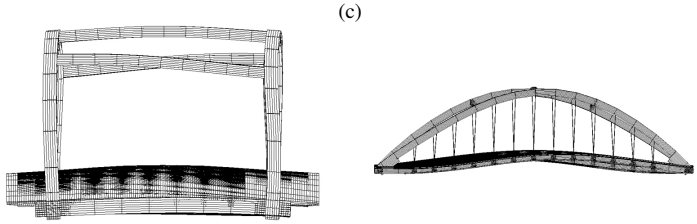

(d)

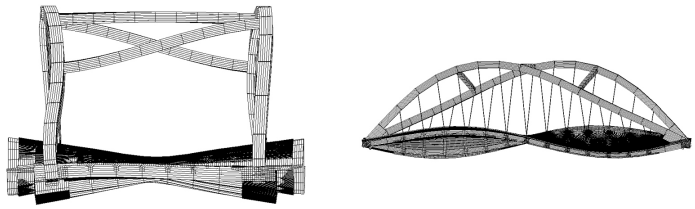

(e)

Fig. 8. [cont.]

3. Results analysis

The impact coefficient is an important parameter for measuring the dynamic effects of bridges when vehicles pass through them. Currently, the guidance for highway heavy transport vehicle load calculation is specified in the “Code for Design of the Municipal Bridge”, which states that when special load calculations are used, impacts are not considered, and neither are pedestrian loads nor non-motorized vehicle loads [18]. Highway heavy transport vehicles are completely different from general load-bearing vehicles. When engineers perform bridge calculations, they often neglect the impact effect, which may deviate from the actual situation. Previous studies have shown that even when vehicles pass through bridges at low speeds, the impact coefficient is still significant, and the impact effect cannot be ignored [17].

There are multiple factors that affect the coupling effect between highway heavy transport vehicles and bridges. This study mainly focuses on factors related to the vehicles and selects the following indicators for extraction and analysis:

1. Vertical displacement of the bridge. This includes the vertical displacement response at the 1/4-span node, mid-span node, 3/4-span node, and the arch crown node.
2. Internal forces of the bridge. This includes the axial force response of suspenders #1, #2, and #3, as shown in Fig. 9; the axial force response at the main arch section of the mid-span; and the axial force response at the arch foot section.

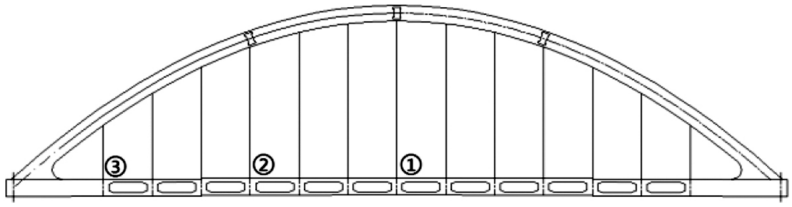

Fig. 9. Positions of suspenders #1, #2, and #3

3.1. Influence of vehicle speed

With bridge stiffness set at 1.0 Kb, bridge Rayleigh damping coefficients $\alpha = 0.3$ and $\beta = 0.001$, and roughness grade taken as B, only considering highway heavy transport loads and assuming the vehicle travels in a single direction while being centered. Due to the uniqueness of suspension systems on heavy transport vehicles, there is currently a lack of understanding of the dynamic characteristics of such suspension systems. Therefore, it is necessary to study the dynamic characteristics of these suspension systems. Based on references from other suspension systems, this study considers the range of variation for first series spring stiffness $0.2k_1 \sim 5k_1$. $5k_1$ is a quite large spring stiffness for a heavy-transport vehicle. However, it is worth mentioning that the loading capacity of heavy vehicles is growing faster, which leading to the increasing of the first series spring stiffness. Our purpose of adopting a wider range of first series spring stiffness is to obtained more general results. The vehicle speed ranges from 1 m/s to 10 m/s (equivalent to 3.6 km/h to 36 km/h). The speed limitation of normal roadways in China is normally 60–80 km/h. In a real heavy-vehicle transport event, the bridge management department demands the vehicle running at a low speed for safety consideration. Hence, the maximum speed of 36 km/h is a reasonable speed for heavy-transport vehicles. The vehicle load varies from 200 t to 700 t (axle loads ranging from 10 t/axle to 30 t/axle).

In this section, the selection working condition is as follows: the heavy transport vehicles are one-way centered, the first series spring stiffness is $1.0k_1$, the first series spring damping is $1.0c_1$, and the vehicle load is 400 t (axle load 20 t/ axis). Six different working conditions were selected, with vehicle speeds at 1 m/s, 2 m/s, 4 m/s, 6 m/s, 8 m/s, and 10 m/s, to study the coupling vibration of the background tied-arch bridge under the influence of highway heavy transport vehicles. The aim is to analyze the change trends of the impact coefficients of the bridge within one vehicle travel cycle.

3.1.1. Displacement impact coefficient of the bridge

Figure 10 shows the variations of vertical displacement amplitudes and vertical displacement impact coefficients at the 1/4-span, mid-span, and 3/4-span under the six working conditions mentioned above. Under all six working conditions, the vertical displacement amplitudes at the 1/4-span, mid-span, and 3/4-span increase with increasing vehicle speed. The influence of speed on the vertical displacement impact coefficients at the 1/4-span, mid-span, and 3/4-span nodes is consistent, with an increase in speed leading to an increase in impact coefficients. At higher vehicle speeds, the impact coefficients are larger, which is extremely detrimental to the bridge's load-bearing capacity. Therefore, it is necessary to appropriately limit the vehicle speed during highway heavy transport. Even when the vehicle travels at very low speeds, the impact effect should still be taken into account and cannot be neglected.

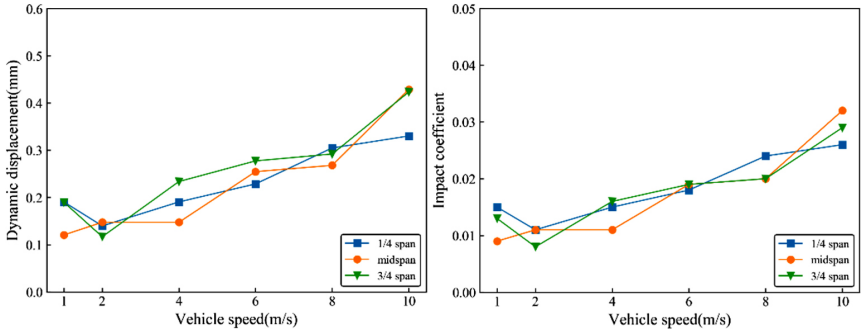

Fig. 10. Influence of vehicle speed on vertical displacement amplitudes and vertical displacement impact coefficients at the 1/4-span, mid-span, and 3/4-span: (a) Vertical displacement amplitudes, (b) Vertical displacement impact coefficients

Fig. 11 shows the variation curves of the arch crown vertical displacement amplitudes and vertical displacement impact coefficients under the six working conditions mentioned

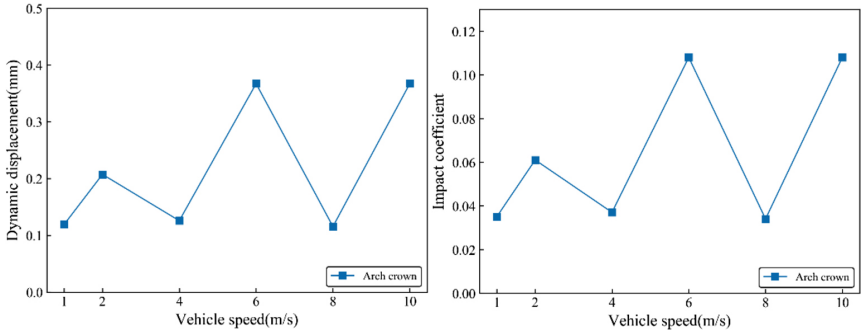

(a) (b)

Fig. 11. Influence of vehicle speed on the arch crown vertical displacement amplitudes and vertical displacement impact coefficients: (a) Vertical displacement amplitudes, (b) Vertical displacement impact coefficients

above. Under these six working conditions, the vertical displacement vibration amplitude of the arch crown varies dramatically. For vehicle speeds of 1 m/s, 4 m/s, and 8 m/s, the vertical displacement vibration amplitude at the arch crown is relatively small. However, for vehicle speeds of 2 m/s, 6 m/s, and 10 m/s, the corresponding displacement amplitudes are larger. The influence of speed on the impact coefficients of the arch crown displacement is significant, but the trend of the impact coefficients does not show a clear pattern. When the vehicle speeds reach 2 m/s, 6 m/s, and 10 m/s, the impact coefficients are relatively high, indicating that the impact effect of arch crown displacement cannot be neglected.

3.1.2. Internal force impact coefficient of the bridge

Figure 12 shows the variations of the axial force amplitudes and axial impact coefficients for suspenders #1, #2, and #3 under the six working conditions mentioned above. The trends of the axial force amplitudes for suspenders #1 and #3 are similar, reaching their maximum values at a speed of 4m/s. The axial force amplitude of suspender #2 initially increases, then decreases, increases again at a speed of 8 m/s, and decreases at a speed of 10 m/s. As for the impact coefficients, the axial impact coefficients of suspenders #1 and #3 first increase, then decrease. At a speed of 4 m/s, the impact coefficient reaches its maximum value, which exceeds the value calculated according to the code [18]. The value calculated according to the code is only 0.05. The maximum impact coefficient of suspender #3 is 0.083, which is 66.6 higher than that calculated according to the code. The impact coefficient of suspender #2 is sensitive to changes in speed but does not show a clear trend. For speeds of 2 m/s and 8 m/s, the impact coefficients are relatively high, measuring 0.036 and 0.041, respectively, slightly lower than the values calculated according to the code.

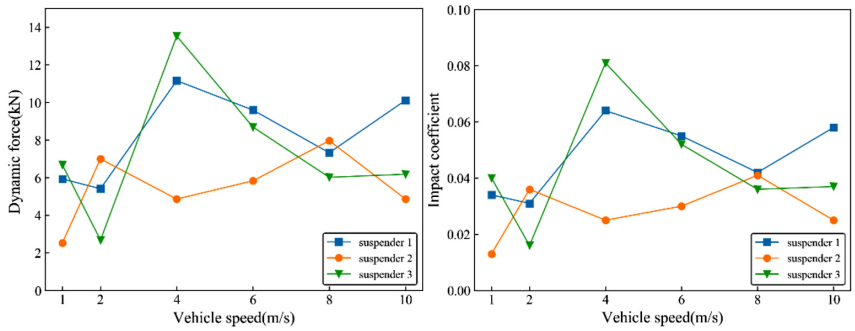

(a) (b)

Fig. 12. Influence of vehicle speed on axial force amplitudes and axial force impact coefficients for suspenders #1, #2, and #3: (a) Axial force amplitudes, (b) Axial force impact coefficients

Figure 13 shows the curves of the axial force amplitudes and axial force impact coefficients for the arch crown and arch foot under the six working conditions. The variation trends of the axial force impact coefficients for the arch crown and arch foot are different, with weak correlation between the two. Overall, the axial force impact coefficient of the arch crown increases with increasing speed and reaches its peak value at 4 m/s, with a maximum impact coefficient

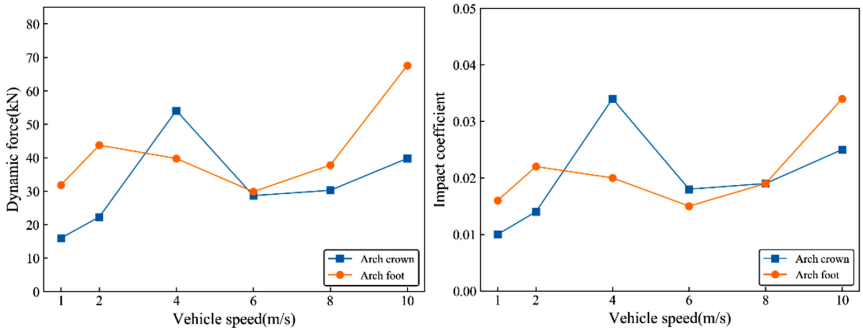

(a) (b)

Fig. 13. Influence of vehicle speed on of axial force amplitudes and axial force impact coefficients for the arch crown and arch foot: (a) Axial force amplitudes, (b) Axial force impact coefficients

of 0.034. The axial force impact coefficient of the arch foot initially decreases, then increases with increasing speed, and reaches its maximum impact coefficient at 10 m/s, equal to 0.034.

Table 4 presents the impact coefficients under different vehicle speeds. Based on the calculation results in Table 4, a range analysis of the changes in each component with speed is performed, leading to the following conclusions:

1. The ranking of the impact coefficients affected by vehicle speed for each component is as follows: displacement impact coefficient of arch crown >axial force impact coefficient of suspender >axial force impact coefficient of arch rib >vertical displacement impact coefficient of longitudinal beam.
2. The ranking of the impact coefficients affected by vehicle speed is as follows: displacement impact coefficient >internal force impact coefficient.

Table 4. Influence of vehicle speed on impact coefficients

Impact coefficient	**Position**	**Vehicle speed**						**Range**
		1 m/s	**2 m/s**	**4 m/s**	**6 m/s**	**8 m/s**	**10 m/s**	
Displacement	1/4-span	0.015	0.011	0.015	0.018	0.024	0.026	0.015
	Mid-span	0.009	0.011	0.011	0.019	0.020	0.032	0.023
	3/4-span	0.013	0.008	0.016	0.019	0.020	0.029	0.021
	Arch crown	0.035	0.061	0.037	0.108	0.034	0.108	0.074
Internal force	Suspender #1	0.034	0.031	0.064	0.055	0.042	0.058	0.033
	Suspender #2	0.013	0.036	0.025	0.030	0.041	0.025	0.028
	Suspender #3	0.040	0.016	0.081	0.052	0.036	0.037	0.065
	Arch crown	0.010	0.014	0.034	0.018	0.019	0.025	0.024
	Arch foot	0.016	0.014	0.020	0.015	0.019	0.034	0.020

3.2. Influence of vehicle load

In this section, the selection working condition is as follows: the heavy transport vehicles are one-way centered, the first series spring stiffness is $1.0k_1$, the first series spring damping is $1.0c_1$. The vehicle speed is 2 m/s. Six operating conditions were selected: 200 t (axial load of 13.3 t/axle), 300 t (axial load of 16.7 t/axle), 400 t (axial load of 20.0 t/axle), 500 t (axial load of 23.3 t/axle), 600 t (axial load of 26.7 t/axle), and 700 t (axial load of 30.0 t/axle). The aim is to analyze the changing trend of the impact coefficient of the bridge under different vehicle loads within one cycle of vehicle operation.

3.2.1. Displacement impact coefficient of the bridge

Figure 14 shows the vertical displacement amplitude and vertical displacement impact coefficient at 1/4 span, mid-span, and 3/4 span nodes as a function of speed. The vertical displacement amplitude of 1/4 span, mid-span, and 3/4 span nodes is not sensitive to changes in vehicle load. The influence of vehicle load variation on the displacement impact coefficient of 1/4 span, mid-span, and 3/4 span nodes is consistent, decreasing with increasing vehicle load. When the vehicle load is small, the impact coefficient is large, but when the vehicle load is large, further increases in vehicle load have a smaller effect on the impact coefficient. In heavy transportation, it is necessary to limit the axle load within a reasonable range. When the vehicle load is small, the vehicle's carrying capacity is not well utilized, and the impact on the bridge is large. When the load is large, although the impact is small, it increases the burden on the bridge and affects the force and durability of the bridge.

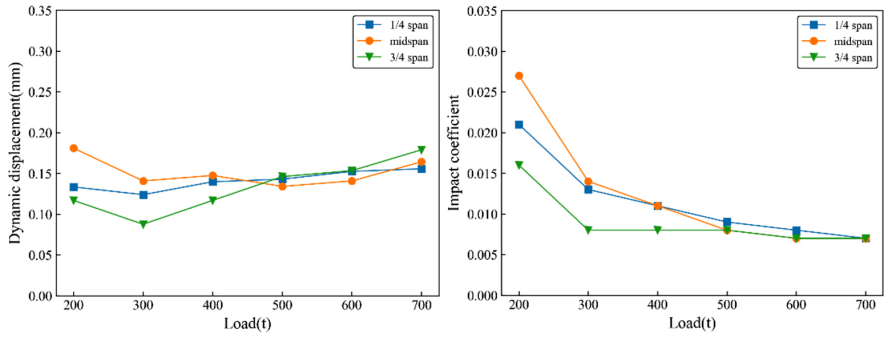

Fig. 14. Influence of vehicle load on vertical displacement amplitudes and vertical displacement impact coefficients at the 1/4-span, mid-span, and 3/4-span: (a) Vertical displacement amplitudes, (b) Vertical displacement impact coefficients

Figure 15 shows the vertical displacement amplitude and vertical displacement impact coefficient of the arch crown as a function of vehicle load. Under the six conditions, the vertical displacement vibration amplitude of the arch crown increases linearly. The displacement impact coefficient decreases when the vehicle load changes from 200 t to 400 t, and stabilizes

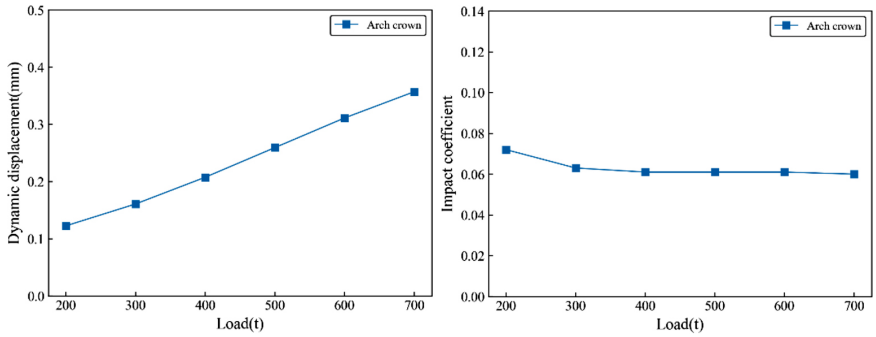

(a) (b)

Fig. 15. Influence of vehicle load on the arch crown vertical displacement amplitudes and vertical displacement impact coefficients: (a) Vertical displacement amplitudes, (b) Vertical displacement impact coefficients

at around 0.060 when the vehicle load exceeds 400 t. In all conditions, the displacement impact coefficient of the arch crown cannot be ignored, and the impact effect needs to be considered in the calculation of heavy transport over the bridge.

3.2.2. Internal force impact coefficient of the bridge

Figure 16 shows the axial force amplitude and impact coefficient of suspenders #1, #2, and #3 as a function of vehicle load. From the figure, it can be observed that the axial force amplitude of suspenders #1, #2, and #3 increases with increasing vehicle load, with suspender #2 having the largest amplitude and suspender #3 having the smallest. The axial impact coefficient of suspenders #1, #2, and #3 decreases with increasing vehicle load. When the vehicle load range is between 200 t and 400 t, the decrease in the impact coefficient is significant, but when the vehicle load exceeds 400 t, the decrease becomes smaller. Among the six operating conditions,

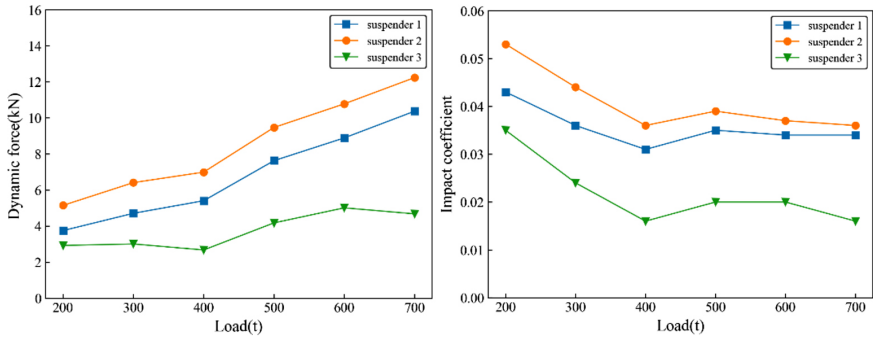

(a) (b)

Fig. 16. Influence of vehicle load on axial force amplitudes and axial force impact coefficients for suspenders #1, #2, and #3: (a) Axial force amplitudes, (b) Axial force impact coefficients

suspender #2 has the largest impact coefficient, while suspender #3 has the smallest. When the vehicle load is 700t (30.0 t per axle), the impact coefficients of suspenders #1, #2, and #3 are 0.034, 0.036, and 0.016 respectively, which are not significantly different from the values at a vehicle load of 400 t.

Figure 17 shows the axial force amplitude and impact coefficient of the arch crown and arch foot as a function of vehicle load. The changing trends of the axial force impact coefficients for the arch crown and arch foot are similar, rapidly decreasing with increasing load, but the rate of decrease becomes smaller when the vehicle load exceeds 400 t.

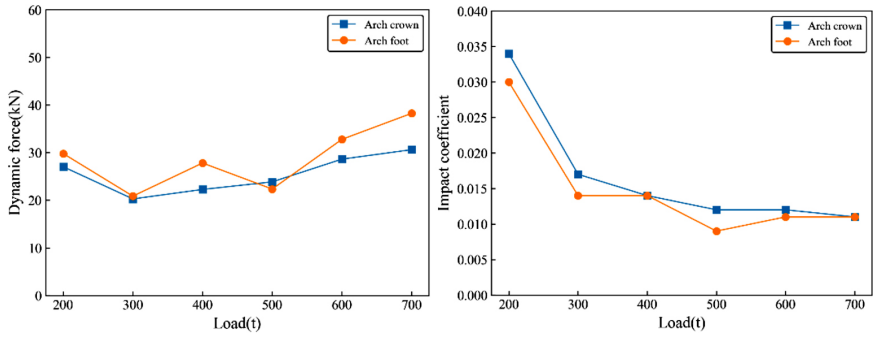

Fig. 17. Influence of vehicle load on of axial force amplitudes and axial force impact coefficients for the arch crown and arch foot: (a) Axial force amplitudes, (b) Axial force impact coefficients

Table 5 presents the impact coefficients under different vehicle loads. Based on the calculation results in Table 5, a range analysis of the changes in each component with vehicle is performed, leading to the following conclusions:

Table 5. Influence of vehicle load on impact coefficients

Impact coefficient	**Position**	**Vehicle speed**						**Range**
		200 t	**300 t**	**400 t**	**500 t**	**600 t**	**700 t**	
Displacement	1/4-span	0.021	0.013	0.011	0.009	0.008	0.007	0.014
	Mid-span	0.027	0.014	0.011	0.008	0.007	0.007	0.020
	3/4-span	0.016	0.008	0.008	0.008	0.007	0.007	0.009
	Arch crown	0.072	0.063	0.061	0.061	0.061	0.060	0.012
Internal force	Suspender #1	0.043	0.036	0.031	0.035	0.034	0.034	0.009
	Suspender #2	0.053	0.044	0.036	0.039	0.037	0.036	0.015
	Suspender #3	0.035	0.024	0.016	0.020	0.020	0.016	0.019
	Arch crown	0.034	0.017	0.014	0.012	0.012	0.011	0.023
	Arch foot	0.030	0.014	0.014	0.009	0.011	0.011	0.019

1. The ranking of the impact coefficients affected by vehicle load for each component is as follows: axial force impact coefficient of arch rib >vertical displacement impact coefficient of longitudinal beam >axial force impact coefficient of suspender >displacement impact coefficient of arch crown.
2. The ranking of the impact coefficients affected by vehicle speed is as follows: internal force impact coefficient >displacement impact coefficient.

4. Conclusions

1. The impact of vehicle speed on the displacement impact coefficient of tied-arch bridge bridges is greater than that of internal force impact coefficient. Different parts of the bridge have inconsistent responses to changes in vehicle speed. At a speed of 4 m/s, the impact coefficient reaches its maximum value.
2. When the vehicle load changes from 200 t to 400 t, the displacement impact coefficient of the tied-arch bridge shows a decreasing trend. When the vehicle load exceeds 400 t, the displacement impact coefficient stabilizes at around 0.060. The axial force impact coefficient of the suspender, arch crown, and arch foot decreases with increasing vehicle load. When the vehicle load range is between 200 t and 400 t, the reduction in impact coefficient is significant. When the vehicle load exceeds 400 t, the reduction is relatively small.
3. The influence of vehicle load on the internal force impact coefficient of tied-arch bridges is greater than that of the displacement impact coefficient. When the vehicle load is large, the impact on the bridge is small, but an excessive increase in vehicle load will increase the burden on the bridge. A load of 400 t is considered a more ideal value.

The main limitation of this research is: The accuracy of the vehicle-bridge coupling model has not been verified by model experiments or field measurement results. We should carry out model experiments or field measurements to improve the accuracy of our model in the future.

Acknowledgements

This study was supported by National Natural Science Foundation of China (52178181) and Hunan Provincial Transportation Science and Technology Project (2018031).

References

[1] Z.D. Chen, “Review and prospect of road bulky transport in China”, *Shanghai Highways*, vol. b11, pp. 175–179, 1999.

[2] P.T. Zhou, Q. Shan, and Y. G. Ye, “Large transport vehicles-bridge coupling dynamics analysis”, *CHINA Measurement & Test*, vol. 43, no. 1, pp. 127-131, 2017.

[3] Y. Huang, “Dynamic performance of bridge piers impacted by heavy trucks”, *Archives of Civil Engineering*, vol. 69, no. 3, pp. 173–185, 2023, doi: 10.24425/ace.2023.146074.

[4] Y. Huang, “On the resistance of concrete hollow thin-walled high piers to rock collisions”, *Archives of Civil Engineering*, vol. 69, no. 3, pp. 187–197, 2023, doi: 10.24425/ace.2023.146075.

[5] H.Q. Zou, H.T. Bai, P. Dai, and Y.M. Nie, "Study on the capacity of large-span steel-box downpass tied-arch bridge to carry large transport vehicles", *Value Engineering*, vol. 42, no. 5, pp. 35–38, 2023, doi: 10.3969/j.issn.1006-4311.2023.05.012.

[6] K.Y. Lu, J.L. Li, Z. Ma, and C.Y. Ma, "Research on rapid assessment technology of bridge safety performance under the condition of heavy transportation", *Construction Quality*, vol. 40, no. 7, pp. 30–34, 2022.

[7] A.A. Malokar and P.L. Naktode, "Study of behavior of locally available bambooas a sustainable reinforcement for concrete structures", *Archives of Civil Engineering*, vol. 68, no. 3, pp. 339–352, 2022, doi: 10.24425/ace.2022.141889.

[8] Y.G. Yuan, G. L. Zhou, W.B. Gao, W.S. Han, T. Wang, and J.F. Wang, "Assessment method for bridges under customized trucks by incorporating safety and serviceability", *Engineering Mechanics*, vol. 38, no. 7, pp. 147–158, 2021, doi: 10.6052/j.issn.1000-4750.2020.07.0490.

[9] Y. Zhang and Z.S. Sun, "Analysis of concrete – filled steel tubular tied – arch bridge under travelling vehicles", *Journal of Railway Science and Engineering*, vol. 13, no. 1, pp. 103–110, 2016, doi: 10.19713/j.cnki.43-1423/u.2016.01.016.

[10] Q.Y. Zeng and P. Yang, "The "set-in-right-position" rule for forming structural matrices and the finite truss element method for space analysis of truss bridges", *Journal of the China Railway Society*, vol. 2, pp. 48–59, 1986.

[11] Q.Y. Zeng, "The Principle of Total Potential Energy with Stationary Value in Elastic System Dynamics", *Journal of Huazhong University of Science and Technology (Natural Science Edition)*, vol. 1, no. 1, pp. 1–3+14, 2000, doi: 10.13245/j.hust.2000.01.001.

[12] B.W. Yin, F. Yang, X.R. Guo, and X.H. He, "Influence of temperature deformation on vehicle£bridge dynamic response of long-span steel box-girder tied-arch bridge", *Journal of Railway Science and Engineering*, vol. 10, no. 6, pp. 21–27, 2013, doi:10.19713/j.cnki.43-1423/u.2013.06.004.

[13] C.S. Cai and S.R. Chen, "Accident assessment of vehicles on long-span bridges in windy environments", *Journal of Wind Engineering and Industrial Aerodynamics*, vol. 92, no. 12, pp. 991–1024, 2004.

[14] Z.H. Zhu, T.T. Zhao, L.D. Wang, H.Q. Xu, and Z.W. Yu, "Stress impact factor of the suspenders of heavy-haul railway arch bridge basedon random vibration model", *Journal of Vibration Engineering*, vol. 30, no. 6, pp. 955–964, 2017, doi: 10.16385/j.cnki.issn.1004-4523.2017.06.009.

[15] P. Lonetti, A. Pascuzzo, and A. Davanzo, "Dynamic Behavior of Tied-Arch Bridges under the Action of Moving Loads", *Mathematical Problems in Engineering*, vol. 2016, art. no. 2749720, 2016, doi: 10.1155/2016/2749720.

[16] J.H. Jang, D.J Min, and M.Y. Kim, "Investigation of Resonance Occurrence Conditions by Dynamic Interaction Analysis between Arch bridge and KTX Trains", *Journal of the Earthquake Engineering Society of Korea*, vol. 20, no. 2, pp. 103–112, 2016, doi: 10.5000/EESK.2016.20.2.103.

[17] G.L. Dai and D.J. Li, *Spatial analysis and design method of bridge structure and its application[M]*. Beijing: China Communications Press, 2001 (in Chinese).

[18] Ministry of Housing and Urban-Rural Development of the People's Republic of China (MOHURD), "Code for design of the municipal bridge", CJJ 11 – 2011.

Received: 2023-12-16, Revised: 2024-03-12